Materials Advances

PAPER

View Article Online
View Journal | View Issue

Check for updates

Cite this: *Mater. Adv.*, 2022, 3, 4641

2D GeP_3 and blue P: promising thermoelectric materials for room- and high-temperature applications†

Lucas Prett Campagna,[a] Marcos Veríssimo-Alves,[a] Debora C. M. Rodrigues,[b] Marcelo F. C. Albuquerque Filho,[b] Pedro Venezuela,[b] Wanderlã L. Scopel[c] and Rodrigo G. Amorim *[a]

Received 6th March 2022,
Accepted 22nd April 2022

DOI: 10.1039/d2ma00265e

rsc.li/materials-advances

Thermoelectric materials have attracted great attention from the research community due to their capability to convert heat into electricity. Among these materials, two-dimensional (2D) systems are potential candidates for thermoelectric applications due to their unique electronic, mechanical and optical properties. In this work, we combine Density Functional Theory and Boltzmann Transport Equation (BTE) calculations to investigate the performance of 2D hexagonal Germanene (Ge), blue Phosphorene (blue P) and GeP_3 as thermoelectric materials. The Seebeck (S), electric conductivity (σ) and thermal electronic conductivity (κ_e) are obtained with the SIESTA and BoltzTraP codes by means of a module especially developed for this aim in combination with the Spglib library, while the lattice thermal conductivity (κ_ℓ) is obtained with the phono3py code. The studied materials have charge carrier concentrations close to 10^{18} cm^{-2}, and blue P displays the largest electric figure of merit ($ZT_e \sim 1.0$), followed by GeP_3 and Ge. Regarding the maximum ZT_e for each of the investigated materials, we find that blue P has a central peak with $ZT_e^{(blueP)} = 1.0$ at $T = 800$ K, Germanene has a pronounced peak with $ZT_e^{(Ge)} = 0.45$ at $T = 340$ K and GeP_3 has two such peaks, with $ZT_e^{GeP_3} = 0.85$ and 0.98 at $T = 300$ K and $T = 10$ K, respectively. For all three compounds, $\kappa_\ell(T)$ in the range $T = 200$–700 K decreases monotonically with increasing T, with ratios $k_\ell^{GeP_3}/k_\ell^{Ge} \sim 10^{-1}$ and $k_\ell^{GeP_3}/k_\ell^{blueP} \sim 10^{-2}$, indicating that the electronic contributions to ZT^{GeP_3} establish its upper bound. Our findings suggest that GeP_3 can be a promising room-temperature thermoelectric material if further tailoring of its electronic properties allow for an increase in ZT_e.

1 Introduction

A large amount of the energy generated globally is wasted due to thermal dissipation, in a scenario where the world's demand increases yearly. One alternative for reducing energy waste is to convert thermal energy into electricity. Thermoelectric materials are thus promising candidates for energy waste reduction due to their capability to convert heat into electricity. This type of material can be also be applied to convert electricity into heat. A measure of the conversion efficiency is the so-called figure of merit, ZT:

$$ZT = \frac{\sigma S^2 T}{\kappa_e + \kappa_\ell}, \quad (1)$$

a dimensionless quantity that ideally should be larger than 1. In eqn (1), κ_e and κ_ℓ are the electronic and lattice contributions, respectively, to the total thermal conductivity, $\kappa = \kappa_e + \kappa_\ell$. An initial indication of whether a candidate thermoelectric material merits further investigation as such is the electronic contribution to the figure of merit, ZT_e:

$$ZT_e = \frac{\sigma S^2 T}{\kappa_e}. \quad (2)$$

For applications, thermoelectric materials must have $ZT > 1$ and while few naturally exhibit such large ZT, it is possible to engineer the electronic and structural properties of materials to specifically increase it. In particular, the groundbreaking proposal that dimensionality reduction would increase ZT due to quantum confinement effects,[1] contributed to a renewed interest in the field, which was further intensified with the synthesis of different 2D materials. A recent review by Ouyang *et al*[2] shows new possibilities for improving thermoelectric performance. Some of the mechanisms listed by the authors to tune the thermoelectric properties of 2D materials are: (i) carrier

[a] *Departamento de Física, ICEx, Universidade Federal Fluminense – UFF, Volta Redonda/RJ, Brazil. E-mail: rgamorim@id.uff.br*
[b] *Instituto de Física, Universidade Federal Fluminense – UFF, Niterói/RJ, Brazil*
[c] *Departamento de Física, Universidade Federal do Espírito Santo – UFES, Vitória/ES, Brazil*

† Electronic supplementary information (ESI) available. See DOI: https://doi.org/10.1039/d2ma00265e

doping, for semiconducting materials; (ii) an increase in the number of layers, which in some cases, such as GeP_3, can lead to an insulator-metal transition, (iii) bandgap tuning by application of strain and (iv) suppression of phonon modes by defects. Other exciting possibilities are the exploitation of phonon coherence and of the effects of topological properties of materials on electrons and phonons.

Snyder *et al.*[3] discussed the way to maximize ZT in semiconductors, where for viable applications the carrier concentrations should be in the range of 10^{18}–10^{21} cm^{-3}. However, as highlighted by Wu *et al.*,[4] for wide bandgap semiconductors such carrier densities are hard to attain, since it is very difficult to dope them. However, for heavily doped narrow bandgap semiconductors, the parameters involved in the expression for ZT – the Seebeck coefficient S, the electric conductivity σ and the thermal conductivity κ – are strongly interdependent.

Since experimental graphene exfoliation,[5] different 2D materials have been explored and successfully synthesized such as Phosphorene,[6,7] Silicene,[8–10] h-BN,[11–13] Germanene,[14–16] Borophene,[17,18] GeP_3,[19] and also 2D hybrid materials Graphene/h-BN[20–22] and MoS_2.[23,24] Monolayers of chalcogenide materials such as GaS, GaSe, and GaTe, semiconductors with indirect bandgap,[25] have already been successfully synthesized on different substrates and their thermoelectric properties have been thoroughly studied. They presented high values of ZT for temperatures below room temperature.

Applications of thermoelectric materials can be devised for many temperature conditions, but a significant impact will be attained for those with high ZT at room temperature, which will allow for energy conversion by many sources of ordinary, daily usage. Moreover, its constituent elements should be environmentally friendly and preferably lightweight. Germanene (Ge), and GeP_3, materials with similar hexagonal lattices, are potentially promising 2D materials for thermoelectric applications at room temperature. Phosphorene (P), another promising 2D thermoelectric material, has three allotropes, the most stable of which is hexagonal blue P, with a lattice similar to those of Ge and GeP_3. All three materials are made of reasonably lightweight chemical elements of low toxicity.

The large 2 eV bandgap and structural stability of blue P make it particularly suitable for high-voltage and high-temperature applications, which led to several studies focusing on its thermoelectric properties. Jain and Alan predicted the thermal conductivity of blue P to be 78 W m^{-1} K^{-1} at 300 K and isotropic, decreasing under biaxial stress.[26] Liao *et al.*[27] explored the effect of electron–phonon coupling on blue P's thermoelectric properties, showing that the power factor is maximum at 200 K, with half of the value of black P. They ascribed it to the larger bandgap of blue P and stronger electron–phonon scattering rates compared to black P. Hu *et al.*[28] studied the thermoelectric properties of black/blue P vertical heterostructures, showing that the reduction of the thermal conductivity associated to van der Waals interaction results in enhanced thermoelectric performance when compared to their monolayer counterparts.

Germanene (Ge), proposed theoretically by Ciraci *et al.*[29] in 2009, has both a high-buckled (HB) and low-buckling (LB) structure, c. van der Waals multilayer germanene was synthesized by Bianco *et al.*,[30] where they claim that single- or few-layer Ge may be obtained by mechanical exfoliation. They also synthesized hydrogen-terminated germanium (GeH), where it was demonstrated that this material is stable up to 348 K and presents slow oxidation under air exposure. Regarding the thermoelectric properties of Ge, Yang *et al.*[31] estimated the upper limit of the figure of merit as ZT_e = 0.41, at room temperature. Peng *et al.*[32] obtained a thermal conductivity κ_ℓ = 2.4 W m^{-1} K^{-1} for Ge at 300 K, decreasing monotonically with increasing temperature.

The bulk phase of GeP_3[33] is known since 1970, but only recently its 2D monolayer structure was proposed.[19] The monolayer phase is semiconducting due to the strong quantum electronic confinement, with a predicted 0.55 eV bandgap. The lower bandgap, in comparison to that of blue P, suggests that it would be more suitable for milder conditions of voltage and temperature, closer to room temperature. Besides GeP_3, the existence of other 2D mono-layered triphosphide materials has been theoretically predicted, such as InP_3[34] and SnP_3.[35] Very recently, Sun *et al.*[36] have investigated the thermoelectric properties of InP_3, GaP_3, SbP_3 and SnP_3 monolayers, predicting high Seebeck coefficients and low thermal conductivities.

In this work, we perform Density Functional Theory (DFT) and Boltzmann Transport Equation (BTE) calculations to explore the thermoelectric properties of 2D hexagonal Ge, GeP_3 and blue P. For each of these materials, the Seebeck coefficient S, the electronic conductivity σ and electronic and lattice thermal conductivities, κ_e and κ_ℓ, respectively, are obtained as a function of the temperature T. With these quantities for each studied system, the figure of merit ZT is explored for different operation temperatures, investigating the role of κ_ℓ in the values of ZT particularly.

2 Methodology

We used an *ab initio* total energy method based on DFT,[37,38] as deployed in the SIESTA[39] and Quantum Espresso[40] codes, for the electronic structure calculations. Thermoelectric properties are calculated using the BTE as implemented in the BoltzTraP code.[41] Since the two codes (DFT and BTE) are independent, we developed a SIESTA module to link them. Details on how to incorporate the module to SIESTA, compilation flags and code validation are discussed in the ESI.† The DFT calculations were performed with the Generalized Gradients Approximation of Perdew, Burke and Ernzerhof (GGA-PBE),[42] norm-conserving Troullier–Martins pseudopotentials,[43] a double-ζ basis set including polarization orbitals (DZP), and the Brillouin Zone (BZ) is sampled according to the Monkhorst–Pack (MP) method.[44] The optimal values for the mesh cutoff and MP sampling grid are 300 Ry and (8 × 8 × 1), respectively. For structural relaxations, the residual force components for each atom are lower than 0.001 eV Å^{-1}.

The lattice thermal conductivity (κ_ℓ) was calculated using a full solution of the linearized phonon Boltzman equation

(LBTE), as implemented in PHONO3PY code.[45,46] A supercell of $6 \times 6 \times 1(2 \times 2 \times 1)$ was employed for Germanene and Phosphorene (GeP_3) with $19 \times 19 \times 1$ q-point sampling meshes. For the supercell approach, the second- and third-order force constant models were calculated with finite displacements of 0.03 Å.

Table 1 Structural parameters for the 2D materials investigated in this study. Numbers in parentheses are results from the literature

	Ge	Blue P	GeP_3
a, b (Å)	8.12 (8.09[a], 7.90[b])	6.63 (6.65[c], 6.56[d])	7.02 (7.09[e], 7.05[f])
δ (Å)	0.71	1.27	

[a] Ref. 47. [b] Ref. 48. [c] Ref. 49. [d] Ref. 50. [e] Ref. 19. [f] Ref. 33.

3 Results

Fig. 1a–c present top views of the fully relaxed 2D geometries for Ge, blue P and GeP_3, respectively. Since the unit cell for GeP_3 contains 8 atoms, we use 2×2 supercells for Ge and blue P, to have the same number of the atoms for each material. Structural parameters for Ge, GeP_3 and blue P are shown in Table 1. Our results are in good agreement with previously published results, with a maximum deviation of in-plane lattice parameter of 1.75% for Ge. All structures are buckled with overall good agreement for the buckling parameter δ, but a sizeable 5% deviation for bond lengths can be seen in GeP_3.

Fig. 2 shows the band structures projected over p-orbitals and their respective distributions of squared electronic group velocity for monolayer Ge, GeP_3 and blue P. Monolayer Ge (Fig. 2a) has semi-metallic character with a Dirac cone at the K point of the Brillouin zone, which is associated with p_z orbitals as reported in the literature.[47] Blue P (Fig. 2c) is a semiconductor character with an indirect bandgap of 2.00 eV, in agreement with the results of Zhu *et al.*[49] The valence band maximum (VBM) and conduction band minimum (CBM) have predominant σ (p_x and p_y) and π (p_z) orbitals, respectively. Monolayer GeP_3 (Fig. 2b) is a semiconductor with a 0.45 eV indirect bandgap and the VBM and CBM are ascribed to p_z orbitals of the Ge atoms, in agreement with results from Jing *et al.*[19] Regarding thermoelectric properties, Fig. 2a–c (right panels) shows that the greatest contribution to $v^2(k)$ is given by the x and y components in essentially similar amounts, while the z contribution is negligible. This is consistent with the fact that electrons are confined to the basal plane of the material, where electronic and thermal conduction will take place.

Fig. 3 shows heat maps for the Seebeck coefficient (S), for the scaled electric conductivity $\sigma' = \sigma/\tau$ and for the electronic thermal conductivity $\kappa_e' = \kappa_e/\tau$, where τ is the electronic scattering time, for each investigated material in the range $-2.0 < E–E_f < +2.0$. For Ge (Fig. 3a), the values of S are very small throughout the whole temperature range, and at 10 K the maximum and minimum values are +0.852 and -0.685 mV K^{-1}, respectively. The positive sign of S in the region $E–E_f < 0.0$ eV indicates electrical transport by holes, while the negative sign in the region $E–E_f > 0.0$ eV indicates that carriers are electrons. At 300 K, our calculations yield $S = \pm 0.14$ mV K^{-1} around E_F, which is consistent with previously published works.[31] In the energy range $-1.0 < E–E_f < +1.0$ eV, $\sigma'(T)$ and $\kappa_e'(T)$ have smaller values in comparison to the rest of the energy range considered. From the graph it can also be inferred that $\kappa_e'(T)$ increases with T, consistent with the results of Chegel *et al.*[51]

At 10 K, blue P has negligible $S(E–E_f)$ values over the energy range $-2.0 < E–E_f < 2.0$ eV except at $E–E_f = \pm 1.0$ eV, as seen in Fig. 3b. Interestingly, these energy values coincide with the CBM and VBM energies, and with the small spread of $S(E–E_f)$ at 10 K, we can infer that $S(E–E_f)$ is a sharp peak. For $10 \leq T \leq 340$ K, the peaks in $S(E–E_f)$ broaden, displaying a sharp edge followed by a slower decay (in absolute value) as one moves towards higher or lower energies, and negligible values between the peak edges. With increasing T, the distance between these edges decreases in an approximate linear fashion up to $T \sim 340$ K and the broadening of the $S(E–E_f)$ peaks increases; on the other hand, $S(E–E_f)$ varies differently for positive and negative $E–E_f$. In the $E–E_f$ range between the sharp edges, both σ' and κ_e' have negligible values, in agreement with the results of ref. 27, and increase outside this energy range.

GeP_3, whose properties are displayed in Fig. 3c, displays a richer behavior, similar in some aspects to that of blue P, but

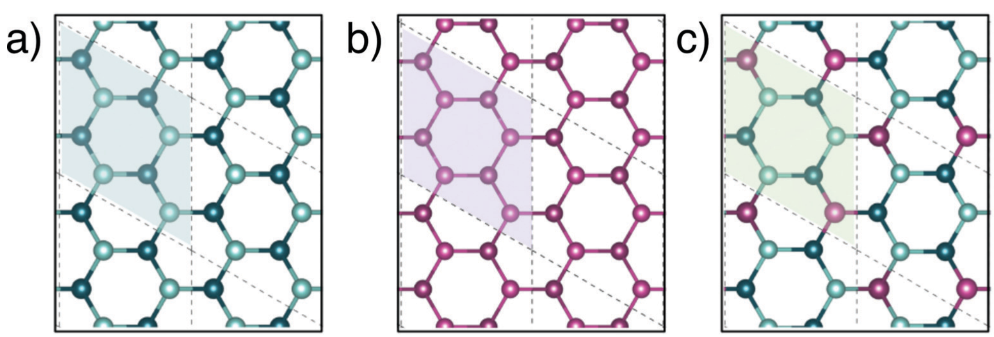

Fig. 1 Top views of fully relaxed atomic structures for (a) Ge, (b) blue P and (c) GeP_3. The shadowed regions depict the unit cell for GeP_3, and supercells for Ge and blue P. Darker and lighter atom shades indicate lower and higher vertical position regarding buckling planes, respectively.

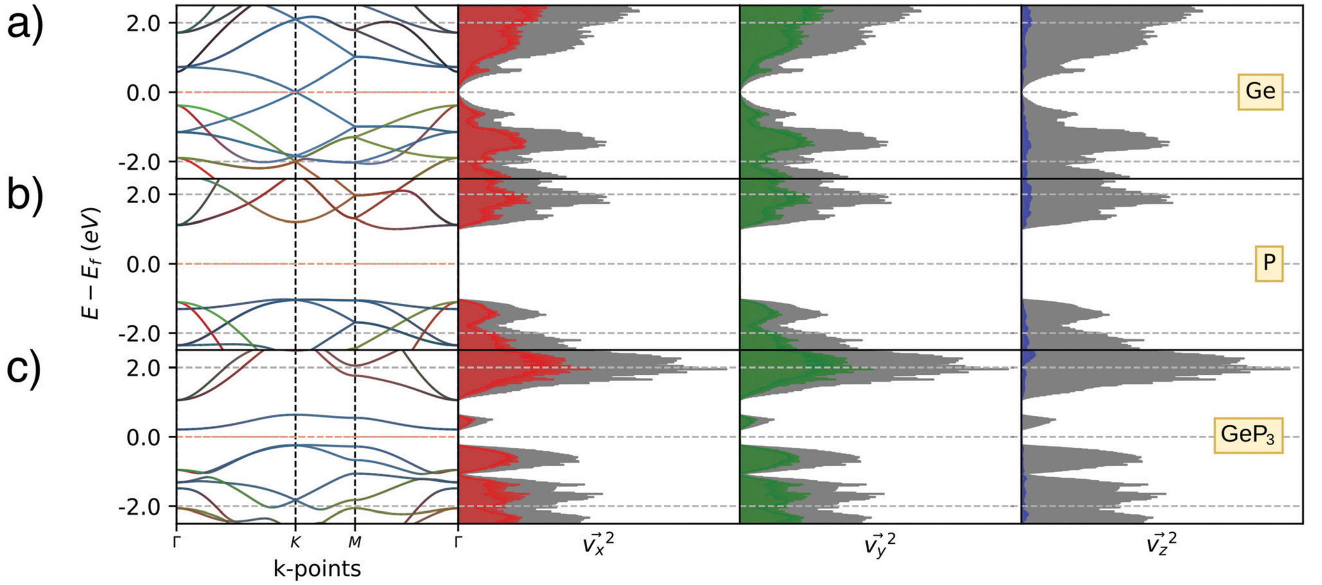

Fig. 2 Band structure projected over p orbitals for (a) Ge; (b) blue P; (c) GeP_3, with the respective squares of group velocity components on the right panels. Red, green, blue and light gray represent v_x^2, v_y^2, v_z^2 and total v^2, respectively. The Fermi level, E_f, is set to zero. The colors red, green and blues also represents the orbitals p_x, p_y and p_z, respectively.

with important differences. At $T = 10$ K, as in the case of blue P, very narrow peaks in $S(E–E_f)$ appear at the energies corresponding to band energy extrema, in the energy range $-0.25 < E–E_f < 1.00$ eV. However, the presence of an isolated conduction band with relatively low dispersion gives rise to two pairs of peaks in $S(E–E_f)$, all of them with a much narrower broadening than those of blue P. The positive peaks are located at the VBM and the maximum of the first CB, while the negative ones are located at the minima of the first and second CB. For increasing T up to 70 K, the distance between adjacent peaks in GeP_3 decreases in an approximately linear fashion, in a similar way to blue P, and remains essentially constant for higher temperatures. For completeness, we mention that there is actually a third pair of peaks in $S(E–E_f)$; however, they occur at $E \leq -1.0$ eV, and are approximately two orders of magnitude less intense than the other peaks. Table 2 summarizes the maximum and minimum values of S, σ' and κ_e', along with the values at which they occur.

For good thermoelectric performance, the material's power factor, $PF = \sigma S^2$, should be maximized and the electrical thermal conductivity, κ_e, minimized. This is a difficult task, however, since high values of σ, in general, imply large κ_e. Fig. 4 shows ZT_e as a function of charge carrier density n for $200 \leq T \leq 700$ K for Germanene, blue P and GeP_3. For Ge (Fig. 4a), two main peaks around $n = 0$ and three smaller ones are observed for higher n. The main peaks broaden and slightly displace towards higher energies with increasing T. The value of ZT_e at 300 K is in agreement with previously published work.[31]

For blue P (Fig. 4b), the curves for ZT_e (T) are very different from those for Ge. Near room temperatures (200–300 K), ZT_e displays a peak with value 1 at $n = 0$, indicating that maximization of ZT_e in this temperature range would not require any doping. At $T \geq 300$ K, however, ZT_e drops to zero, rising sharply for minimal values of electron ($n < 0$) or hole ($n > 0$) doping, broadening with rising T. Thus, our results suggest that blue P would still be a good thermoelectric material in a broad range of T with a minimal amount of electron doping.

In turn, the ZT_e curves of GeP_3 (Fig. 4c) display a behaviour intermediate to those of Ge and blue P. First, we note that ZT_e now displays two intense pairs of peaks, reflecting that $S(E–E_f)$ is large for two different energy ranges. Remarkably, while ZT_e shows sharp drops to zero at all values of T, it would not require any doping for its maximization, since the first drop occur at values slightly below $n = 0$. As T rises, the peaks broaden as for blue P, with a small decrease in their maximum values.

Fig. 5 shows the maximum value of ZT_e, $ZT_{e,max}$ (left y-axis, blue) and the temperature T at which it occurs (right y-axis, orange) as a function of the excess carrier concentration n, for the three materials studied. It also shows $ZT_{e,max}$ for a fixed temperature of 300 K (purple dash-dotted line), for considerations on room-temperature performance. From this figure, we can infer the temperatures at which the material presents a maximum in $ZT_{e,max}$ and the amount of n- or p-doping required to achieve it, thus serving as an aid in tailoring the material for obtaining maximum thermoelectric performance. In the analysis that follows, we shall refer to the temperatures at which the maxima of $ZT_{e,max}$ occur as working temperatures (T_w) of the three materials studied. The amount of doping, n, will be given in units of 10^{18} carriers cm^{-2} and T_w will be given in K. Table 3 lists the above mentioned values.

$ZT_{e,max}^{(Ge)}(n,T)$ displays four broad peaks. Despite having T_w at room temperature ranges, it indicates that Ge will perform poorly as a thermoelectric material at all temperatures, even if spurious doping happens, for range 200–800 K since $ZT_{e,max}^{(Ge)}$ at

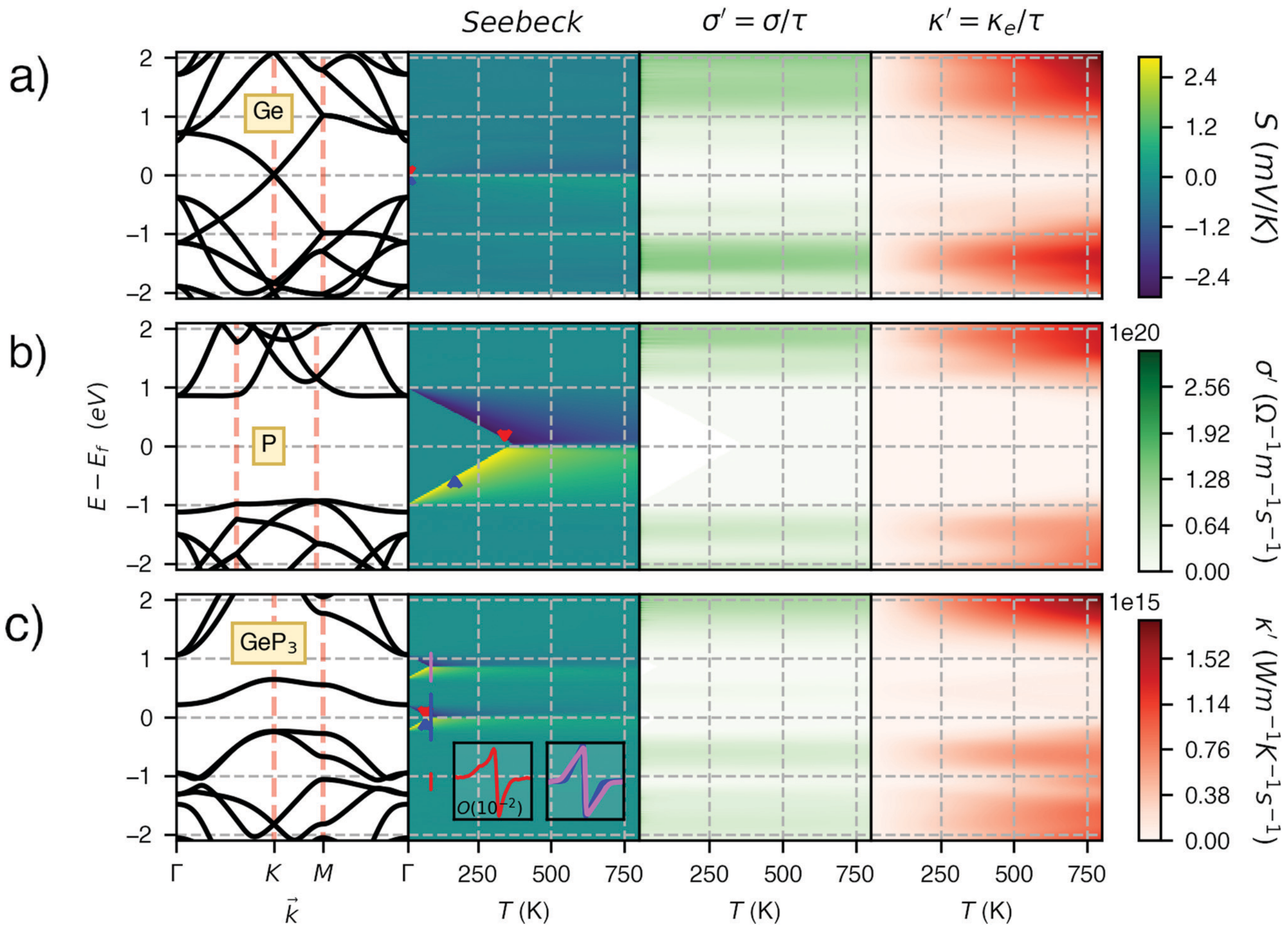

Fig. 3 The band structure $E(k)$, the Seebeck coefficient S, scaled electrical conductivity $\sigma' = \sigma/\tau$ and electronic thermal conductivity $\kappa'_e = \kappa_e/\tau$ for (a) Ge, (b) blue P and (c) GeP_3. The Fermi level is set at zero. The red and blue arrows indicate the location of the maximum and minimum values, respectively, of S for each material.

Table 2 Maximum and minimum values of S (mV K^{-1}), σ' (Ω^{-1} m^{-1} s^{-1}) and κ'_e (W m^{-1} K^{-1} s^{-1}). Numbers in parenthesis are the temperature T (K) at which they occur

	S_{max}	S_{min}	σ'_{max}	σ'_{min}	$\kappa'_{e,max}$	$\kappa'_{e,min}$
Ge	+0.852 (10)	−0.685 (10)	1.13×10^{17} (10)	7.96×10^{14} (10)	3.68×10^{9} (10)	1.87×10^{9} (10)
Blue P	3.062 (340)	−2.809 (170)	3.23×10^{5} (340)	1.38×10^{4} (170)	8.70×10^{2} (340)	2.21 (170)
GeP_3	2.872 (70)	−2.869 (70)	2.45×10^{-2} (70)	9.85×10^{-3} (70)	1.42×10^{1} (70)	5.73×10^{0} (70)

T_w is well below 1. In contrast, peaks in $ZT^{(P)}_{e,max}$ (Fig. 5b) occur mostly at T = 800 K for all carrier concentrations, except at $n \geq 11.5$, and the $ZT^{(P)}_e(n,T)$ curve displays a broad cusp shape and two others where $ZT^{(P)}_e(n,T)$ is close to zero. Although blue P has a high T_w, which could affect n significantly, the cusp is very broad, suggesting it could have acceptable thermoelectric performance even if spurious doping should happen. While $T^{(P)}_w$ = 800 K, the data in Table 3 show an acceptable value for ZT_e at T = 300 K, and from Fig. 5b it can be inferred that blue P could also perform almost equally well in thermoelectric devices at this temperature.

$ZT^{(GeP)_3}_{e,max}(n, T)$, in turn, displays a complex behaviour, with two broad cusp-shaped peaks of potential interest for thermoelectric applications, and a second pair of broader, but lower, pair of peaks occurring at high values of n. Table 3 shows that GeP_3 will not be able to operate optimally at room temperature, since these two values of $ZT^{(GeP)_3}_{e,max}(n, T)$ occur well below it. However, the values of ZT_e (n = 0, T = 300 K) are comparable to

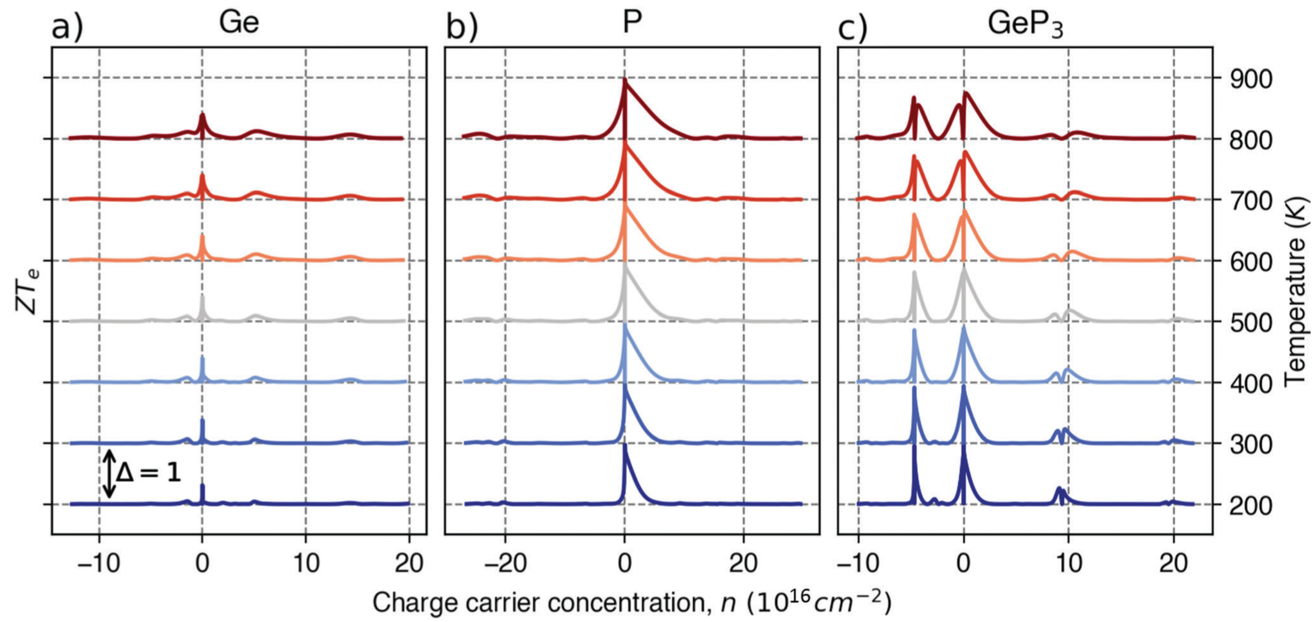

Fig. 4 The electronic figure of merit at different temperatures for: (a) germanene, (b) blue P and (c) GeP_3.

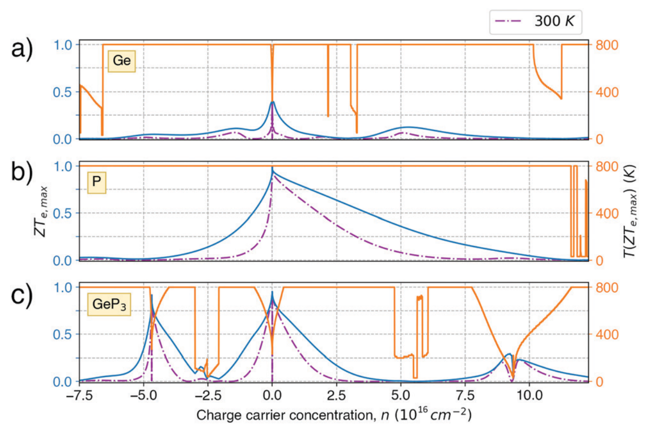

Fig. 5 Maximum value of ZT_e ($ZT_{e,max}$, full blue line) and the temperature at which it occurs (T ($ZT_{e,max}$), orange full line) as a function of charge carrier concentration n for the three materials studied for (a) germanene; (b) blue P and (c) GeP_3. ZT_e (T = 300 K) curves are also presented in dash-dotted purple lines.

Table 3 Values for $ZT_{e,max}$ and the corresponding (n,T) and T_w. For comparison, values for $ZT_{e,max}$ (T = 300 K) are also given, with the corresponding n

	$ZT_{e,max}$	n (10^{16} cm^{-2})	T (K)	T_w (K)	$ZT_e^{(T=300K)}$	n (10^{16} cm^{-2})
Ge	0.05	−4.7	800	325	0.01	−4.9
	0.11	−1.4	800		0.07	−1.5
	0.40	0.0	325		0.38	0.0
	—	—	—		0.02	1.8
	0.12	5.3	800		0.06	5.1
P	0.03	−7.2	800	800	0.01	−6.7
	1.00	0.0	800		0.92	0.0
	—	—	—		0.02	9.3
GeP_3	0.90	−4.7	270	300	0.74	−4.7
	0.16	−2.8	94		0.28	−4.7
	0.95	0.0	229		0.84	0.1
	0.29	9.2	112		0.20	9.0
	0.23	9.6	265		0.23	9.6

those for blue P. In particular, $ZT_e^{(GeP)_3}$ (n = 0, T = 300 K) is only 9% lower than that of blue P at the same temperature. As remarked earlier, ZT_e is at best a first indicator of thermoelectric performance. In actual applications, lattice vibrations are likely to have a non-negligible contribution, and it must be explicitly considered. Using eqn (2), eqn (1) can be rewritten as

$$ZT = \frac{ZT_e}{1 + \frac{\kappa_\ell}{\kappa_e' \tau}}. \quad (3)$$

Therefore, the smaller $\kappa_\ell/\kappa_e'\tau$, the better the thermoelectric performance.

To estimate the contribution of the lattice thermal conductivity, we have calculated $\kappa_\ell(T)$ in the range 200–800 K, shown in Fig. 6. Table 4 summarizes our calculated values of κ_e' and κ_ℓ, along with relaxation times τ, averaged for the zigzag and armchair directions,[52–54] and the calculated total ZT at T = 300 K, for electron and hole transport. In ref. 52–54, the authors determine the scattering times in the deformation potential approximation, and therefore they do not consider the polar optical phonon contribution to the conductivities. Within this approximation, Table 4 clearly shows that GeP_3 has superior thermal lattice properties, when compared to blue P; the latter, however, has lower scattering times. Therefore, both GeP_3 and blue P have comparable $ZT^{(el,h)}$ values, with a slightly higher value for hole transport in blue P. Since $T_w^{(P)}$ is 800 K, it will display peak performance at high-temperature applications, although it would also have comparable (but slightly lower)

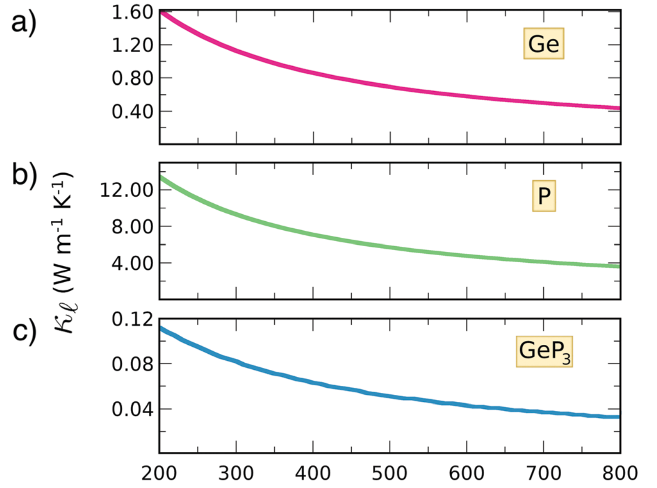

Fig. 6 Thermal conductivity as a function of temperature for (a) germanene; (b) blue P and (c) GeP_3.

Table 4 Values for lattice and electronic thermal conductivities, κ_e' and κ_ℓ, relaxation times for electron and hole transport averaged for zigzag and armchair directions (taken from ref. 52 for Ge, ref. 53 for P and ref. 54 for GeP_3), for all three materials studied at T = 300 K. Thermal lattice conductivities are given in W m^{-1} K^{-1}, thermal electronic conductivities are in units of 10^{13} and relaxation times are given in ps

	κ_e'	κ_ℓ	$\tau_{avg}^{(el)}$	$\tau_{avg}^{(h)}$	$ZT^{(el)}$	$ZT^{(h)}$
Ge	1.167	1.12	5.325	5.520	0.40	0.40
P	2.617	9.3	0.051	0.465	0.86	0.91
GeP_3	0.048	0.08	0.175	0.755	0.83	0.84

performance for room-temperature applications. In turn, GeP_3 would perform better in room-temperature applications, given its T_w = 300 K.

4 Conclusions

We have combined DFT and Boltzmann Transport Equation calculations to explore the thermal properties of 2D Ge, blue P and GeP_3. This combination was possible by the development of a module for the SIESTA code using the Spglib library to output the calculation results in a format suitable for post-processing with BoltzTraP. A GitHub link for downloading the module code, along with instructions and compilation flags for incorporation in SIESTA, are provided in the ESI.†

Our electronic structure results suggest that 2D Ge is metallic, while blue P and GeP_3 are semiconductors, with a literature good agreement. Optimal charge carrier concentrations for thermoelectric operation are in the range 10^{16} cm^{-2} for all three materials. Our calculations also show that GeP_3 has the lowest κ_ℓ in the temperature range T = 200–800 K, and Ge and blue P have κ_ℓ one and two orders of magnitude higher, respectively, in the same temperature range.

$ZT_{e,max}^{(Ge)}$ displays many broad peaks for a wide range of excess charge carrier concentrations n. However, as expected for a metallic material, all peaks are much lower than 1, which implies that Ge is unsuitable for thermoelectric applications. $ZT_{e,max}^{(P)}$ displays one broad but pronounced peak at $n \approx 0$ and T = 800 K, being only slightly below 1 at T = 300 K. $ZT_{e,max}^{(GeP)_3}$, on the other hand, presents two broad peaks at n = 0 and n = -4.7×10^{16} carriers cm^{-2} for T = 229 and 270 K, respectively, being also slightly under 1 for these values of n and T. Nevertheless, at T = 300 K and n = 0.1 × 10^{16} carriers cm^{-2}, $ZT_e^{(T=300\text{ K})} = 0.84$.

An interesting feature suggested by our calculations is that the dominant part of ZT for GeP_3 and blue P is electronic: despite having κ_ℓ differing by three orders of magnitude, $\kappa_e \ll \kappa_\ell$ for both materials and, as suggested by eqn (3), ZT is reduced essentially to ZT_e. Therefore, there could be room for further improvement of ZT_e for both GeP_3 and blue P through strain and defect engineering. The effects of strain on $ZT_e^{(GeP_3,P)}$ will be the subject of a future publication.

Conflicts of interest

There are no conflicts to declare.

Acknowledgements

The authors acknowledge financial support from the Brazilian agencies CAPES, CNPq, FAPES and the LNCC (SCAFMat2), CENAPAD-SP for computer time. WLS and RGA thank for financial support from CNPq (301648/2017-4 and 421227/2018-4) and (2535/2017-1, 437182/2018-5 and 313076/2020-0), respectively. RGA also acknowledge financial support from FAPERJ grant numbers E-26/010.101126/2018, E-26/210.077/2022 and E-26/202.699/2019. DCMR also thank FAPERJ grant numbers E-26/202.085/2020 and E-26/202.086/2020. This study was financed in part by the Coordenação de Aperfeiçoamento de Pessoal de Nível Superior – Brasil (CAPES) – Finance Code 001.

Notes and references

1 L. D. Hicks and M. S. Dresselhaus, *Phys. Rev. B: Condens. Matter Mater. Phys.*, 1993, **47**, 12727–12731.
2 Y. Ouyang, Z. Zhang, D. Li, J. Chen and G. Zhang, *Ann. Phys.*, 2019, **531**, 1800437.
3 G. J. Snyder and E. S. Toberer, *Materials for sustainable energy: a collection of peer-reviewed research and review articles from Nature Publishing Group*, 2011, pp. 101–110.
4 J. Wu, Y. Chen, J. Wu and K. Hippalgaonkar, *Adv. Electron. Mater.*, 2018, **4**, 1800248.
5 K. S. Novoselov, A. K. Geim, S. V. Morozov, D.-E. Jiang, Y. Zhang, S. V. Dubonos, I. V. Grigorieva and A. A. Firsov, *Science*, 2004, **306**, 666–669.
6 H. Liu, A. T. Neal, Z. Zhu, Z. Luo, X. Xu, D. Tománek and P. D. Ye, *ACS Nano*, 2014, **8**, 4033–4041.
7 R. N. Pedrosa, R. G. Amorim and W. L. Scopel, *Nanotechnology*, 2020, **31**, 275201.

8 S. Cahangirov, M. Topsakal, E. Aktürk, H. S. Ahin and S. Ciraci, *Phys. Rev. Lett.*, 2009, **102**, 236804.
9 P. Vogt, P. De Padova, C. Quaresima, J. Avila, E. Frantzeskakis, M. C. Asensio, A. Resta, B. Ealet and G. Le Lay, *Phys. Rev. Lett.*, 2012, **108**, 155501.
10 R. G. Amorim and R. H. Scheicher, *Nanotechnology*, 2015, **26**, 154002.
11 K. K. Kim, A. Hsu, X. Jia, S. M. Kim, Y. Shi, M. Hofmann, D. Nezich, J. F. Rodriguez-Nieva, M. Dresselhaus, T. Palacios and J. Kong, *Nano Lett.*, 2012, **12**, 161–166.
12 M. S. Bresnehan, G. R. Bhimanapati, K. Wang, D. W. Snyder and J. A. Robinson, *ACS Appl. Mater. Interfaces*, 2014, **6**, 16755–16762.
13 X. Chen, J. F. Dobson and C. L. Raston, *Chem. Commun.*, 2012, **48**, 3703–3705.
14 S. Jiang, S. Butler, E. Bianco, O. D. Restrepo, W. Windl and J. E. Goldberger, *Nat. Commun.*, 2014, **5**, 3389.
15 E. Bianco, S. Butler, S. Jiang, O. D. Restrepo, W. Windl and J. E. Goldberger, *ACS Nano*, 2013, **7**, 4414–4421.
16 M. E. Dávila and G. Le Lay, *Sci. Rep.*, 2016, **6**, 1–9.
17 G. Silvestre, W. L. Scopel and R. Miwa, *Nanoscale*, 2019, **11**, 17894–17903.
18 T. L. G. Cabral, L. T. S. De Miranda, D. C. de Melo Rodrigues, F. A. de Souza, W. L. Scopel and R. G. Amorim, *J. Phys.: Condens. Matter*, 2021, **34**, 095502.
19 Y. Jing, Y. Ma, Y. Li and T. Heine, *Nano Lett.*, 2017, **17**, 1833–1838.
20 G. Lu, T. Wu, P. Yang, Y. Yang, Z. Jin, W. Chen, S. Jia, H. Wang, G. Zhang and J. Sun, *et al.*, *Adv. Sci.*, 2017, **4**, 1700076.
21 F. A. De Souza, R. G. Amorim, W. L. Scopel and R. H. Scheicher, *Nanotechnology*, 2016, **27**, 365503.
22 F. A. L. de Souza, G. Sivaraman, J. Hertkorn, R. G. Amorim, M. Fyta and W. L. Scopel, *J. Mater. Chem. A*, 2019, **7**, 8905–8911.
23 G. Sivaraman, F. A. de Souza, R. G. Amorim, W. L. Scopel, M. Fyta and R. H. Scheicher, *J. Phys. Chem. C*, 2016, **120**, 23389–23396.
24 A. Perez, R. G. Amorim, C. E. P. Villegas and A. R. Rocha, *Phys. Chem. Chem. Phys.*, 2020, **22**, 27053–27059.
25 B. P. Bahuguna, L. Saini, R. O. Sharma and B. Tiwari, *Phys. Chem. Chem. Phys.*, 2018, **20**, 28575–28582.
26 A. Jain and A. J. McGaughey, *Sci. Rep.*, 2015, **5**, 1–5.
27 Z. Liu, J. Morales-Ferreiro and T. Luo, *Appl. Phys. Lett.*, 2018, **113**, 063903.
28 R. Hu, Z. Zhou, C. Sheng, L. Wang, J. Liu, S. Han and H. Liu, *Phys. Chem. Chem. Phys.*, 2020, **22**, 22390–22398.
29 S. Cahangirov, M. Topsakal, E. Aktürk, H. Sahin and S. Ciraci, *Phys. Rev. Lett.*, 2009, **102**, 236804.
30 E. Bianco, S. Butler, S. Jiang, O. D. Restrepo, W. Windl and J. E. Goldberger, *ACS Nano*, 2013, **7**, 4414–4421.
31 K. Yang, S. Cahangirov, A. Cantarero, A. Rubio and R. D'Agosta, *Phys. Rev. B: Condens. Matter Mater. Phys.*, 2014, **89**, 125403.
32 B. Peng, H. Zhang, H. Shao, Y. Xu, G. Ni, R. Zhang and H. Zhu, *Phys. Rev. B*, 2016, **94**, 245420.
33 P. Donohue and H. Young, *J. Solid State Chem.*, 1970, **1**, 143–149.
34 N. Miao, B. Xu, N. C. Bristowe, J. Zhou and Z. Sun, *J. Am. Chem. Soc.*, 2017, **139**, 11125–11131.
35 S. Sun, F. Meng, H. Wang, H. Wang and Y. Ni, *J. Mater. Chem. A*, 2018, **6**, 11890–11897.
36 Z. Sun, K. Yuan, Z. Chang, S. Bi, X. Zhang and D. Tang, *Nanoscale*, 2020, **12**, 3330–3342.
37 P. Hohenberg and W. Kohn, *Phys. Rev.*, 1964, **136**, B864.
38 W. Kohn and L. J. Sham, *Phys. Rev.*, 1965, **140**, A1133.
39 J. M. Soler, E. Artacho, J. D. Gale, A. García, J. Junquera, P. Ordejón and D. Sánchez-Portal, *J. Phys.: Condens. Matter*, 2002, **14**, 2745.
40 P. Giannozzi, *et al.*, *J. Phys.: Condens. Matter*, 2009, **21**, 395502.
41 G. K. Madsen and D. J. Singh, *Comput. Phys. Commun.*, 2006, **175**, 67–71.
42 J. P. Perdew, K. Burke and M. Ernzerhof, *Phys. Rev. Lett.*, 1996, **77**, 3865.
43 N. Troullier and J. L. Martins, *Phys. Rev. B: Condens. Matter Mater. Phys.*, 1991, **43**, 1993.
44 H. J. Monkhorst and J. D. Pack, *Phys. Rev. B: Solid State*, 1976, **13**, 5188.
45 K. Mizokami, A. Togo and I. Tanaka, *Phys. Rev. B*, 2018, **97**, 224306.
46 A. Togo, L. Chaput and I. Tanaka, *Phys. Rev. B: Condens. Matter Mater. Phys.*, 2015, **91**, 094306.
47 S. J. Zaveh, M. Roknabadi, T. Morshedloo and M. Modarresi, *Superlattices Microstruct.*, 2016, **91**, 383–390.
48 M. Derivaz, D. Dentel, R. Stephan, M.-C. Hanf, A. Mehdaoui, P. Sonnet and C. Pirri, *Nano Lett.*, 2015, **15**, 2510–2516.
49 Z. Zhu and D. Tománek, *Phys. Rev. Lett.*, 2014, **112**, 176802.
50 W. Zhang, H. Enriquez, Y. Tong, A. Bendounan, A. Kara, A. P. Seitsonen, A. J. Mayne, G. Dujardin and H. Oughaddou, *Small*, 2018, **14**, 1804066.
51 R. Chegel and S. Behzad, *Sci. Rep.*, 2020, **10**, 1–12.
52 X.-S. Ye, Z.-G. Shao, H. Zhao, L. Yang and C.-L. Wang, *RSC Adv.*, 2014, **4**, 21216–21220.
53 J. Xiao, M. Long, X. Zhang, J. Ouyang, H. Xu and Y. Gao, *Sci. Rep.*, 2015, **5**, 9961.
54 B. Zeng, M. Long, X. Zhang, Y. Dong, M. Li, Y. Yi and H. Duan, *J. Phys. D: Appl. Phys.*, 2018, **51**, 235302.